Journal of Computational and Applied Mathematics 407 (2022) 114015

Contents lists available at ScienceDirect

Journal of Computational and Applied Mathematics

journal homepage: www.elsevier.com/locate/cam

High order unconditionally energy stable RKDG schemes for the Swift–Hohenberg equation☆

Hailiang Liu [a], Peimeng Yin [b,*]

[a] Iowa State University, Department of Mathematics, Ames, IA 50011, USA
[b] Multiscale Methods and Dynamics Group, Computer Science and Mathematics Division, Oak Ridge National Laboratory, Oak Ridge, Tennessee 37831, USA

ARTICLE INFO

Article history:
Received 22 June 2021
Received in revised form 26 September 2021

MSC:
65N12
65N30
35K35

Keywords:
Gradient flows
RK method
EQ approach
DG methods
Energy stability

ABSTRACT

We propose unconditionally energy stable Runge–Kutta (RK) discontinuous Galerkin (DG) schemes for solving a class of fourth order gradient flows including the Swift–Hohenberg equation. Our algorithm is geared toward arbitrarily high order approximations in both space and time, while energy dissipation remains preserved for arbitrary time steps and spatial meshes. The method integrates a penalty free DG method for spatial discretization with a multi-stage algebraically stable RK method for temporal discretization by the energy quadratiztion (EQ) strategy. The resulting fully discrete DG method is proven to be unconditionally energy stable. By numerical tests on several benchmark problems we demonstrate the high order accuracy, energy stability, and simplicity of the proposed algorithm.

1. Introduction

In this paper, we are concerned with arbitrarily high order numerical approximations to a class of fourth order gradient follows,

$$u_t = -\mathcal{L}^2 u - \Phi'(u),\ x \in \Omega,\ t > 0, \tag{1.1}$$

where $\mathcal{L} = -(\Delta + a)$ is a second-order operator with a physical parameter a and Φ is a nonlinear function bounded from below. The model equation (1.1) governs the evolution of a scalar time-dependent unknown $u = u(x,t)$ in a convex domain $\Omega \subset \mathbb{R}^d$ and it describes important physical processes in nature. Typical examples of (1.1) include the Swift–Hohenberg equation [1] and the extended Fisher–Kolmogorov equation [2,3].

We consider boundary conditions of form

$$\text{(i) } u \text{ is periodic;} \quad \text{or (ii) } \partial_{\mathbf{n}} u = \partial_{\mathbf{n}} \Delta u = 0, \quad x \in \partial\Omega, \tag{1.2}$$

☆ The work of Peimeng Yin is sponsored by the Office of Advanced Scientific Computing Research, U.S. Department of Energy, and performed at the Oak Ridge National Laboratory, which is managed by UT-Battelle, LLC under Contract No. DE-AC05-00OR22725 with the U.S. Department of Energy. The United States Government retains and the publisher, by accepting the article for publication, acknowledges that the United States Government retains a non-exclusive, paid-up, irrevocable, world-wide license to publish or reproduce the published form of this manuscript, or allow others to do so, for United States Government purposes. The Department of Energy will provide public access to these results of federally sponsored research in accordance with the DOE Public Access Plan (http://energy.gov/downloads/doe-public-access-plan).

* Corresponding author.
E-mail addresses: hliu@iastate.edu (H. Liu), yinp@ornl.gov (P. Yin).

https://doi.org/10.1016/j.cam.2021.114015
0377-0427/

where **n** stands for the unit outward normal to the boundary $\partial\Omega$. With such boundary conditions, Eq. (1.1) indeed features the energy dissipation property:

$$\frac{d}{dt}\mathcal{E}(u) = -\int_{\Omega} |u_t|^2 dx \leq 0, \tag{1.3}$$

where the free energy

$$\mathcal{E}(u) = \int_{\Omega} \frac{1}{2}(\mathcal{L}u)^2 + \Phi(u)dx. \tag{1.4}$$

The model equation is nonlinear, its analytical solution is intractable. Hence designing accurate, efficient, and energy stable algorithms to solve it becomes essential. This energy dissipation law as a fundamental property of (1.1) has been explored in high order numerical approximations [4–6]. It was shown to be crucial to eliminate numerical results that are not physical. In this paper, we construct, analyze, and numerically validate unconditionally energy stable and arbitrarily high order schemes to solve the above model problem, for which we use discontinuous Galerkin (DG) methods for spatial discretization, and high order Runge–Kutta (RK) methods for time discretization.

In the literature, there has been rapid development of different methods for simulating gradient flow models including (1.1), see e.g., [7–18]. They vary either in the spatial discretization or the time discretization, while the latter typically emphasizes preserving the energy dissipation property with no or mild time step restrictions. Let us briefly discuss the existing works closely related to what we do here.

DG spatial discretization. It is known that for equations containing higher order spatial derivatives, DG discretization entails subtle difficulties in defining numerical fluxes. Several approaches have been developed to deal with the difficulties, including the local DG (LDG) methods [19–21], the mixed symmetric interior penalty (SIPG) methods [22–24], the direct DG methods (DDG) [25–27], and the ultra-weak DG [28]. To avoid certain drawbacks of these methods, a penalty free DG method was introduced in [29], where the symmetric structure of the model (1.1) is essentially used. This method still inherits the advantages of the usual DG methods, [30–33], its distinct feature lies in numerical fluxes without using any interior penalty. This is the spatial discretization we shall follow in this work.

EQ reformulation and time discretization. To keep the energy stability for gradient flow models, several time discretization techniques are available in the literature, including the convex splitting [12,13], and the stabilization approach [14,15]. The former leads to nonlinear schemes, and the later often imposes restrictions on nonlinear terms in the model. The energy quadratization (EQ) approach introduced in [16,17] turned to be more general in the sense that it could be applied to a class of gradient flow models. Based on the idea of EQ, the scalar auxiliary variable (SAV) approach was introduced later in [18], where linear systems only with constant coefficients need to be solved. Several extensions of EQ and SAV have been further explored in [34–37]. Earlier EQ based schemes are mostly up to 2nd order accurate in time, until recent works [38,39], where the EQ formulation is combined with the Runge–Kutta methods to achieve high order in time schemes. Note that their schemes are fully nonlinear so that the solution existence and uniqueness are not guaranteed for large time steps. This issue is further addressed in [40] in which the obtained schemes are unconditionally energy stable and linear. However, existing EQ based schemes such as [16,17,38–40] use mainly finite-difference or spectral methods for spatial discretization. New difficulties arise when coupling EQ with the DG discretization, which is the main focus of this work.

Integration of DG with EQ. Integration of EQ formulation with DG for solving (1.1) began with [5], where up to 2nd order (in time) IEQ-DG schemes were introduced. These schemes are shown to be unconditionally energy stable. A key point for the success in the scheme formulation is that the auxiliary energy variable is updated in pointwise manner, and then projected back into the DG space. This strategy of constructing the IEQ-DG schemes was further extended to solve the Cahn–Hilliard equation [41], where the spatial discretization is based on the DDG method [25,26]. However, all these EQ based DG schemes are no more than second order in time.

1.1. Present investigation

We begin with a semi-discrete DG scheme of from (2.4), which is an ODE system coupled with an algebraic relation, and the energy dissipation law is well preserved at this semi-discrete level. The results in [5] show that 2nd order (in time) DG schemes can be made unconditionally energy stable. One interesting question about this semi-DG formulation remains unanswered by previous studies: can we identify even higher order time discretization that is still unconditionally energy stable?

In order to answer this question, we augment the DG formulation to a 'linearized' ODE system by introducing an auxiliary function, which is not necessarily in the DG space. We further apply a multi-stage RK method for temporal discretization. Through a careful analysis we are able to establish that the resulting fully discrete RKDG method is unconditionally energy stable if we adopt an algebraically stable RK time discretization. Such algebraically stable RK class has been previously explored for energy stable time-discretization of some gradient flow models, see, e.g., [38–40,42].

We would like to point out that the special form of the underlying semi-discrete DG formulation requires new techniques in both the scheme construction and the proof of the energy stability. For instance, in order to ensure the explicit update of the EQ auxiliary variable, a spatial projection is essentially used in each stage to project it back

into the DG space. This helps to reduce the computational cost while fulfilling the explicit update of the auxiliary variable in DG space. In addition, the semi-discrete DG scheme in the mixed formulation involves an intermediate function $q = -(\Delta + a)u$, which plays an essential role for avoiding the use of any penalty parameter on interior cell boundaries [29]. In the proof of the energy dissipation property, several novel techniques are designed to handle the underlying DG formulation, for which u and q are independently approximated in DG space. To the best of our knowledge, the RKDG method presented here provides the first unconditionally energy stable schemes of arbitrarily high order for (1.1) within the DG framework.

1.2. Our contribution

In this paper, we propose new Runge–Kutta DG schemes to solve (1.1), which at their core integrate a penalty free DG discretization with an algebraically stable RK time discretization. The following consists of our main contributions.

- We prove that the RKDG method features a discrete energy dissipation law for any time steps, hence called unconditionally energy stable.
- We conduct experiments on benchmark examples to assess the performance of the proposed method. First, we present numerical results to show the high order of spatial and temporal accuracy of the RKDG method, and the energy dissipating property of numerical solutions. Second, we conduct experiments on some two-dimensional pattern formation problems, all of which demonstrate the good performance of the RKDG algorithm.

The common feature of gradient flow models is that the dynamics is driven by minimizing a free energy. There are other gradient flows such as the classical Allen–Cahn equation [43] and Cahn–Hilliard equation [44]. Our method can be readily adapted to the Allen–Cahn equation. For the Cahn–Hilliard equation, instead of (2.4), the semi-discrete DG formulation introduced in [41] may be used as a basis for developing a similar high order RKDG method.

1.3. Organization

In Section 2, we formulate a unified semi-discrete DG method for the gradient flow (1.1) subject to two different boundary conditions. In Section 3, we present RKDG schemes, and establish the energy dissipation law at the discrete level. We also present an RKDG algorithm following a prediction–correction procedure. In Section 4, we verify the good performance of the RKDG algorithm using several benchmark numerical examples. Finally some concluding remarks are given in Section 5.

2. Spatial DG discretization

We derive mathematical formulation for our method. We begin with rewriting (1.1) as a mixed form

$$\begin{cases} u_t = & -\mathcal{L}q - \Phi'(u), \\ q = & \mathcal{L}u. \end{cases} \tag{2.1}$$

Such reformulation is not unique, the symmetric feature of (2.1) is essential for our DG method without the use of any interior penalty [29]. Let us recall some conventions of the DG discretization introduced in [29]. Let the domain Ω be a union of shape regular meshes $\mathcal{T}_h = \{K\}$, with the mesh size $h_K = \mathrm{diam}\{K\}$ and $h = \max_K h_K$. We denote the set of the interior interfaces by Γ^0, the set of all boundary faces by Γ^∂, and the discontinuous Galerkin finite element space by

$$V_h = \{v \in L^2(\Omega) \ : \ v|_K \in P^k(K), \ \forall K \in \mathcal{T}_h\},$$

where $P^k(K)$ denotes the set of polynomials of degree no more than k on element K. If the normal vector on the element interface $e \in \partial K_1 \cap \partial K_2$ is oriented from K_1 to K_2, then the average $\{\cdot\}$ and the jump $[\cdot]$ operator are defined by

$$\{v\} = \frac{1}{2}(v|_{\partial K_1} + v|_{\partial K_2}), \quad [v] = v|_{\partial K_2} - v|_{\partial K_1},$$

for any function $v \in V_h$, where $v|_{\partial K_i}$ $(i = 1, 2)$ is the trace of v on e evaluated from element K_i.

The penalty free DG discretization of (2.1) on each element, following [29], is of the form

$$\int_K u_{ht}\phi dx = -\int_K \nabla q_h \cdot \nabla\phi dx + \int_{\partial K} \widehat{\partial_\nu q_h}\phi + (q_h - \widehat{q_h})\partial_\nu\phi ds + \int_K \left(aq_h - \Phi'(u_h)\right)\phi dx, \tag{2.2a}$$

$$\int_K q_h\psi dx = \int_K \nabla u_h \cdot \nabla\psi dx - \int_{\partial K} \widehat{\partial_\nu u_h}\psi + (u_h - \widehat{u_h})\partial_\nu\psi ds - \int_K au_h\psi dx, \tag{2.2b}$$

for $u_h, \ q_h \in V_h$ with test functions $\phi, \ \psi \in V_h$. Here, ν is the outward normal direction to ∂K for each K. On cell interfaces $e \in \partial K \bigcap \Gamma^0$, central numerical fluxes

$$\widehat{\partial_\nu q_h} = \{\partial_\nu q_h\}, \ \widehat{q_h} = \{q_h\}, \ \widehat{\partial_\nu u_h} = \{\partial_\nu u_h\}, \ \widehat{u_h} = \{u_h\} \tag{2.3}$$

are adopted.

Summation of (2.2) over all elements $K \in \mathcal{T}_h$ leads to a unified DG formulation, which is to find $(u_h(\cdot,t), q_h(\cdot,t)) \in V_h \times V_h$ such that

$$(u_{ht}, \phi) = -G(q_h, \phi) - (\Phi'(u_h), \phi), \tag{2.4a}$$

$$(q_h, \psi) = G(u_h, \psi), \tag{2.4b}$$

for all $\phi,\ \psi \in V_h$. The precise form of $G(\cdot,\cdot)$ depending on the types of boundary conditions is given as follows:

$$\begin{aligned} G(w,v) = &\sum_{K\in\mathcal{T}_h}\int_K (\nabla w\cdot\nabla v - awv)\,dx + \sum_{e\in\Gamma^0}\int_e (\{\partial_\nu w\}[v] + [w]\{\partial_\nu v\})\,ds \\ &+ \frac{\theta}{2}\int_{\Gamma^\partial} (\{\partial_\nu w\}[v] + [w]\{\partial_\nu v\})\,ds, \end{aligned} \tag{2.5}$$

where $\theta = 1$ for (i) of (1.2) and $\theta = 0$ for (ii) of (1.2). Note that for periodic case (i) the left boundary and the right boundary are considered as same, for which we use the factor $1/2$ to avoid recounting. The initial data for u_h is taken as the piecewise L^2 projection, denoted by $u_h(x,0) = \Pi u_0(x)$.

The remarkable property of the above DG scheme is that the discrete energy of form

$$\mathcal{E}(u_h, q_h) := \frac{1}{2}\|q_h\|^2 + \int_\Omega \Phi(u_h)dx \tag{2.6}$$

admits a discrete dissipation law [29]:

$$\frac{d}{dt}\mathcal{E}(u_h, q_h) = -\int_\Omega |u_{ht}|^2 dx \le 0. \tag{2.7}$$

3. Time discretization

This section is devoted to arbitrarily higher order time discretization of the DG formulation (2.4). First, we choose C_0 so that $\Phi(w) + C_0 > 0,\ \forall w \in \mathbb{R}$, and introduce

$$H(w) = \frac{\Phi'(w)}{\sqrt{\Phi(w) + C_0}}. \tag{3.1}$$

The IEQ reformulation of (2.4) requires to find $(u_h(\cdot,t), q_h(\cdot,t)) \in V_h \times V_h$ and U such that

$$(u_{ht}, \phi) = -G(\phi, q_h) - (H(u_h)U, \phi), \tag{3.2a}$$

$$(q_h, \psi) = G(u_h, \psi), \tag{3.2b}$$

$$U_t = \frac{1}{2}H(u_h)u_{ht}, \tag{3.2c}$$

for all $\phi, \psi \in V_h$. The initial data for the above scheme is chosen as

$$u_h(x,0) = \Pi u_0(x), \quad U(x,0) = \sqrt{\Phi(u_0(x)) + C_0},$$

where Π denotes the piecewise L^2 projection into V_h. Note that $U \notin V_h$.

There are two steps involved in the time discretization of (3.2). First, we utilize the numerical solutions of u_h for $t \le t_n$ to obtain a high order approximation u_h^*, and replace the semi-discrete DG scheme (3.2) by

$$(u_{ht}, \phi) = -G(\phi, q_h) - \left(H(u_h^*)U, \phi\right), \tag{3.3a}$$

$$(q_h, \psi) = G(u_h, \psi), \tag{3.3b}$$

$$U_t = \frac{1}{2}H(u_h^*)u_{ht}. \tag{3.3c}$$

This linear scheme can be further solved in $t \in (t_n, t_{n+1}]$ by a high order ODE solver. We should point out that the above treatment does not destroy the energy dissipation property. Since for the modified energy functional

$$E(q_h, U) = \frac{1}{2}\|q_h\|^2 + \|U\|^2 = \mathcal{E}(u_h, q_h) + C_0|\Omega| \tag{3.4}$$

still satisfies

$$\frac{d}{dt}E(q_h, U) = -\int_\Omega |u_{ht}|^2 dx \le 0.$$

Recall that for ODE of from $y_t = f(t,y)$, the general s-stage Runge–Kutta (RK) method has the form

$$y^{n+1} = y^n + \tau\sum_{i=1}^{s} b_i k_i,$$

where

$$k_i = f(t_n + c_i\tau, y^n + \tau \sum_{j=1}^{s} a_{ij}k_j), \quad i = 1, \ldots, s.$$

Here for consistency the RK coefficients satisfy $c_i = \sum_{j=1}^{s} a_{ij}$ and $\sum_{i=1}^{s} b_i = 1$. For the convenience in applying the RK method to the semi-discrete DG schemes, we introduce the operator L_h by

$$(L_h v, \phi) = G(v, \phi) \quad \forall \phi \in V_h. \tag{3.5}$$

3.1. RKDG method

Applying an s-stage RK time discretization to semi-discrete scheme (3.3), we obtain the following RKDG method. For given u_h^n, U^n and $u_{ih}^{n,*} = u_h^*(x, t_n + c_i\tau)$, we find

$$(u_h^{n+1}, q_h^{n+1}, U_h^{n+1}) \in V_h \times V_h \times V_h$$

by

$$u_h^{n+1} = u_h^n + \tau \sum_{i=1}^{s} b_i \xi_{ih}, \tag{3.6a}$$

$$q_h^{n+1} = L_h u_h^{n+1}, \tag{3.6b}$$

$$U^{n+1} = U_h^n + \tau \sum_{i=1}^{s} b_i l_i, \tag{3.6c}$$

$$U_h^{n+1} = \Pi U^{n+1}, \tag{3.6d}$$

where $\xi_{ih} \in V_h$ and l_i are determined by

$$(\xi_{ih}, \phi) = -G(\tilde{q}_{ih}, \phi) - \left(H(u_{ih}^{n,*})\tilde{U}_i, \phi\right), \quad i = 1, 2, \ldots, s \tag{3.7a}$$

$$(\tilde{q}_{ih}, \psi) = G(\tilde{u}_{ih}, \psi), \quad \forall \phi, \psi \in V_h, \tag{3.7b}$$

$$l_i = \frac{1}{2} H(u_{ih}^{n,*})\xi_{ih}, \tag{3.7c}$$

and

$$\tilde{u}_{ih} = u_h^n + \tau \sum_{j=1}^{s} a_{ij}\xi_{jh}, \tag{3.8a}$$

$$\tilde{U}_i = U_h^n + \tau \sum_{j=1}^{s} a_{ij} l_j. \tag{3.8b}$$

Definition 3.1 (*Algebraically Stable RK Method [45]*)**.** A RK method is algebraically stable if the RK coefficients satisfy stability conditions

$$b_i \geq 0, \quad i = 1, 2, \ldots, s, \quad \text{and} \quad M \text{ is positive semi-definite}, \tag{3.9}$$

where M is a symmetric matrix with elements

$$M_{ij} = b_i a_{ij} + b_j a_{ji} - b_i b_j. \tag{3.10}$$

Next, we show that the above RKDG scheme is unconditionally energy stable.

Theorem 3.1. *The RKDG method with its RK coefficients satisfying the stability condition (3.9) is uniquely solvable for any $\tau > 0$ and unconditionally energy stable in the sense that*

$$E_h^{n+1} \leq E_h^n - \tau \sum_{i=1}^{s} b_i \|\xi_{ih}\|^2, \tag{3.11}$$

where the energy

$$E_h^n := E(q_h^n, U_h^n) = \frac{1}{2}\|q_h^n\|^2 + \|U_h^n\|^2.$$

Proof. In order to prove (3.11), we use $\|U_h\| \le \|U\|$ to obtain

$$E_h^{n+1} - E_h^n \le \frac{1}{2}(\|q_h^{n+1}\|^2 - \|q_h^n\|^2) + (\|U^{n+1}\|^2 - \|U_h^n\|^2)$$

and estimate two terms on the right, respectively. First we have

$$\begin{aligned}\frac{1}{2}\left(\|q_h^{n+1}\|^2 - \|q_h^n\|^2\right) =& (q_h^{n+1} - q_h^n, q_h^{n+1}) - \frac{1}{2}\|q_h^{n+1} - q_h^n\|^2 \\ =& G(u_h^{n+1} - u_h^n, q_h^{n+1}) - \frac{1}{2}\|q_h^{n+1} - q_h^n\|^2 \\ =& \tau\sum_{i=1}^{s} b_i G(q_h^{n+1}, \xi_{ih}) - \frac{1}{2}\|q_h^{n+1} - q_h^n\|^2.\end{aligned}$$

Note that from ((3.6)ab), ((3.7)b) and ((3.8)a), we have

$$\begin{aligned}q_h^{n+1} =& L_h u_h^{n+1} = L_h u_h^n + \tau\sum_{j=1}^{s} b_j L_h \xi_{jh}, \\ \tilde{q}_{ih} =& L_h \tilde{u}_{ih} = L_h u_h^n + \tau\sum_{j=1}^{s} a_{ij} L_h \xi_{jh}.\end{aligned}$$

This gives

$$q_h^{n+1} = \tilde{q}_{ih} + \tau\left(\sum_{j=1}^{s} b_j L_h \xi_{jh} - \sum_{j=1}^{s} a_{ij} L_h \xi_{jh}\right),$$

which implies

$$G(q_h^{n+1}, \xi_{ih}) = G(\tilde{q}_{ih}, \xi_{ih}) + \tau\left(\sum_{j=1}^{s} b_j G(L_h\xi_{jh}, \xi_{ih}) - \sum_{j=1}^{s} a_{ij} G(L_h\xi_{jh}, \xi_{ih})\right). \tag{3.12}$$

Setting $\phi = -\xi_{ih}$ in ((3.7)a), we have

$$\begin{aligned}-\|\xi_{ih}\|^2 =& G(\tilde{q}_{ih}, \xi_{ih}) + \left(H(u_{ih}^{n,*})\tilde{U}_i, \xi_{ih}\right) \\ =& G(\tilde{q}_{ih}, \xi_{ih}) + 2(\tilde{U}_i, l_i),\end{aligned} \tag{3.13}$$

where we have used ((3.7)c) in the last step. Combining (3.13) with (3.12) gives

$$G(q_h^{n+1}, \xi_{ih}) = -\|\xi_{ih}\|^2 - 2(\tilde{U}_i, l_i) + \tau\left(\sum_{j=1}^{s} b_j G(L_h\xi_{jh}, \xi_{ih}) - \sum_{j=1}^{s} a_{ij} G(L_h\xi_{jh}, \xi_{ih})\right).$$

Further, using ((3.6)ab), we obtain

$$\begin{aligned}\frac{1}{2}\|q_h^{n+1} - q_h^n\|^2 =& \frac{1}{2}\left(L_h u_h^{n+1} - L_h u_h^n, L_h u_h^{n+1} - L_h u_h^n\right) \\ =& \frac{1}{2}\tau^2\sum_{i,j=1}^{s} b_i b_j \left(L_h\xi_{ih}, L_h\xi_{jh}\right) \\ =& \frac{1}{2}\tau^2\sum_{i,j=1}^{s} b_i b_j G(\xi_{ih}, L_h\xi_{jh}).\end{aligned}$$

For the second term we use ((3.6)c) to obtain

$$\begin{aligned}\|U^{n+1}\|^2 - \|U_h^n\|^2 =& 2(U^{n+1}, U^{n+1} - U_h^n) - \|U^{n+1} - U_h^n\|^2 \\ =& 2(U^{n+1}, \tau\sum_{i=1}^{s} b_i l_i) - (U^{n+1} - U_h^n, U^{n+1} - U_h^n) \\ =& 2\tau\sum_{i=1}^{s} b_i (U^{n+1}, l_i) - \tau^2\sum_{i,j=1}^{s} b_i b_j (l_i, l_j).\end{aligned}$$

Putting together all these estimates,

$$\begin{aligned} E_h^{n+1} - E_h^n \le & -\frac{1}{2}\tau^2 \sum_{i,j=1}^{s} b_i b_j G(\xi_{ih}, L_h\xi_{jh}) - \tau^2 \sum_{i,j=1}^{s} b_i b_j (l_i, l_j) \\ & + \tau \sum_{i=1}^{s} b_i G(q_h^{n+1}, \xi_{ih}) + 2\tau \sum_{i=1}^{s} b_i (U^{n+1}, l_i) \\ \le & -\tau^2 \sum_{i,j=1}^{s} b_i b_j (l_i, l_j) - \tau \sum_{i=1}^{s} b_i \|\xi_{ih}\|^2 + 2\tau \sum_{i=1}^{s} b_i (U^{n+1} - \tilde{U}_i, l_i) \\ & + \tau^2 \left(\frac{1}{2} \sum_{i,j=1}^{s} b_i b_j G(L_h\xi_{jh}, \xi_{ih}) - \sum_{i,j=1}^{s} b_i a_{ij} G(L_h\xi_{jh}, \xi_{ih}) \right). \end{aligned}$$

Subtracting ((3.8)b) from ((3.6)c) gives

$$U^{n+1} - \tilde{U}_i = \tau \sum_{j=1}^{s} b_j l_j - \tau \sum_{j=1}^{s} a_{ij} l_j.$$

Hence

$$2\tau \sum_{i=1}^{s} b_i (U^{n+1} - \tilde{U}_i, l_i) = 2\tau^2 \left(\sum_{i,j=1}^{s} b_i b_j (l_i, l_j) - \sum_{i,j=1}^{s} b_i a_{ij} (l_i, l_j) \right).$$

Combining the results above, we have

$$\begin{aligned} E_h^{n+1} - E_h^n \le & -\tau \sum_{i=1}^{s} b_i \|\xi_{ih}\|^2 - \frac{\tau^2}{2} \sum_{i,j=1}^{s} M_{ij}(L_h\xi_{ih}, L_h\xi_{jh}) - \tau^2 \sum_{i,j=1}^{s} M_{ij}(l_i, l_j) \\ \le & -\tau \sum_{i=1}^{s} b_i \|\xi_{ih}\|^2, \end{aligned}$$

where we have used (3.9).

It is left to prove the unique solvability of the fully discrete scheme, for which it suffices to prove the linear scheme admits only a zero solution if $u_h^n = 0$ and $U^n = 0$. In fact from $E_h^n = 0$, the energy dissipation inequality above tells that

$$\frac{1}{2}\|q_h^{n+1}\|^2 + \|U^{n+1}\|^2 + \tau \sum_{i=1}^{s} b_i \|\xi_{ih}\|^2 + \frac{\tau^2}{2} \sum_{i,j=1}^{s} M_{ij}(L_h\xi_{ih}, L_h\xi_{jh}) + \tau^2 \sum_{i,j=1}^{s} M_{ij}(l_i, l_j) \le 0.$$

This therefore ensures that

$$q_h^{n+1} = 0, U^{n+1} = 0, \quad i = 1, \dots, s,$$

and $b_i\xi_{ih} = 0$ for $i = 1 \cdots s$, so $u_h^{n+1} = \tau \sum_{i=1}^{s} b_i \xi_{ih} = 0$. □

Remark 3.1. System (3.7) may be put as a closed linear system as

$$\begin{aligned} (\xi_{ih}, \phi) + \frac{\tau}{2} \sum_{j=1}^{s} a_{ij} \left(H(u_{ih}^{n,*})^2 \xi_{jh}, \phi \right) + G(\tilde{q}_{ih}, \phi) = & -\left(H(u_{ih}^{n,*}) U_h^n, \phi \right), \\ \tau \sum_{j=1}^{s} a_{ij} G(\xi_{jh}, \psi) - (\tilde{q}_{ih}, \psi) = & -G(u_h^n, \psi), \end{aligned}$$

where the first equation is obtained by plugging ((3.8)b) as well as ((3.7)c) into ((3.7)a), and the second equation is obtained by plugging ((3.8)a) into ((3.7)b).

To implement the RKDG method, we need to prepare u_h^*, hence $u_{ih}^{n,*}$. For $n = 0$, we take

$$u_h^0 = \Pi u_0, \quad u_{ih}^{0,*} = u_h^0.$$

For $n \ge 1$, we construct a Lagrangian interpolating polynomial u_h^* based on $s + 2$ points:

$$(t_{n-1}, u_h^{n-1}), (t_{n-1} + c_i\tau, \tilde{u}_{ih}), (t_n, u_h^n),$$

and set

$$u_{ih}^{n,*} = u_h^*(x, t_n + c_i\tau).$$

However, two drawbacks might show up with this simple extrapolation: (i) when s is large, interpolating polynomials may be highly oscillatory, leading to instability or inaccuracy of the extrapolation from $[t_{n-1}, t_n]$ to $(t_n, t_{n+1}]$; (ii) the order of accuracy of the interpolation can be lower than the order of the RK method, putting another restriction on the overall accuracy of the resulting scheme.

3.2. RKDG algorithm

Let $U_h^*(x, t)$ be the Lagrangian interpolation polynomial based on the interpolating points

$$(t_{n-1}, U_h^{n-1}), (t_{n-1} + c_i\tau, \tilde{U}_{ih}) \text{ and } (t_n, U_h^n), i = 1, 2, \ldots, s.$$

Here, $\tilde{U}_{ih} = \Pi\tilde{U}_i$ is the piecewise L^2 projection of $\tilde{U}_i$ in ((3.8)b) from $(t_{n-1}, t_n]$.

The RKDG algorithm goes as follows: Given u_h^n, U^n, $u_h^*(x, t_n + c_i\tau)$ and $U_h^*(x, t_n + c_i\tau)$, $i = 1, 2, \ldots, s$, we explore a two-step prediction–correction.

Prediction Set $\tilde{u}_{ih}^0 = u_h^*(x, t_n + c_i\tau)$, $\tilde{U}_{ih}^0 = U_h^*(x, t_n + c_i\tau)$, we iteratively solve

$$\left(\xi_{ih}^{m+1}, \phi\right) = -G(\tilde{q}_{ih}^{m+1}, \phi) - \left(H(\tilde{u}_{ih}^m)\tilde{U}_{ih}^m, \phi\right), \quad m = 0, 1, \ldots, \tag{3.14a}$$

$$(\tilde{q}_{ih}^{m+1}, \psi) = G(\tilde{u}_{ih}^{m+1}, \psi), \quad \forall\phi, \psi \in V_h, \tag{3.14b}$$

and

$$\tilde{u}_{ih}^{m+1} = u_h^n + \tau\sum_{j=1}^{s} a_{ij}\xi_{jh}^{m+1}, \tag{3.15a}$$

$$l_i^{m+1} = \frac{1}{2}H(\tilde{u}_{ih}^{m+1})\xi_{ih}^{m+1}, \tag{3.15b}$$

$$\tilde{U}_i^{m+1} = U_h^n + \tau\sum_{j=1}^{s} a_{ij}l_j^{m+1}, \tag{3.15c}$$

$$\tilde{U}_{ih}^{m+1} = \Pi\tilde{U}_i^{m+1}. \tag{3.15d}$$

We stop the iteration and set $u_{ih}^{n,*} = \tilde{u}_{ih}^L$, where $L \geq 0$ is either a priori given integer, or $L \geq 1$ such that $\max_i \|\tilde{u}_{ih}^L - \tilde{u}_{ih}^{L-1}\|_\infty < Tol$.

Correction With the predicted $u_{ih}^{n,*}$, we apply RKDG to update the numerical solution, and also set

$$\tilde{U}_{ih} = \Pi\tilde{U}_i$$

for the update in the next time step.

Remark 3.2. The energy (1.4) when discretized in spatial variable by the DG method becomes the energy (2.6). The semi-discrete DG scheme (2.4) satisfies a discrete energy dissipation law. The closeness of these versions of energy is expected due to the high order of accuracy of the DG scheme. Such dissipation law still holds true at the fully discrete level by the IEQ time discretization, yet the modified energy (3.4) can deviate from (2.6) due to the use of auxiliary variable U. However, with an appropriate number of iterations (L) in the prediction step, they can be very close. A numerical example (Example 4.4) is given to demonstrate how the prediction step helps to reduce the difference of the two energy expressions. This energy deviation issue has also been recently addressed in [46,47] using relaxation techniques.

4. Numerical results

In this section, we numerically test the orders of convergence of the proposed RKDG schemes. Further, we apply the schemes to the 2D Swift–Hohenberg equation in order to recover some known patterns, while we also verify the unconditional energy stability at the same time. Before going further two remarks are in order:

Remark 4.1 (*The Choice of C_0*)**.** To ensure the energy stability it suffices to take $C_0 > -\inf\Phi(u)$. We observe that a larger C_0 can help to reduce the spatial projection error when associated with the DG discretization. For example, let ΠU_0 be the piecewise L^2 projection of U_0 in V_h based on P^1 polynomials, then the projection error is known as

$$\|U_0 - \Pi U_0\| = Ch|U_0|_{H^1(\Omega)}, \tag{4.1}$$

where C is independent of h and U_0. Note that

$$|U_0|^2_{H^1(\Omega)} = \sum_{K\in\Omega}\int_K \left(\frac{\Phi'(u_0)}{\sqrt{\Phi(u_0)+C_0}}\right)^2 |\nabla u_0|^2 dx,$$

from which we see that a larger C_0 will reduce the total error.

Remark 4.2 (*The Choice of the RK Method*)**.** A variety of algebraically stable RK methods have been introduced in the literature, see, e.g., [45]. Here we recall three methods in the form of the Butcher tableau. Qin and Zhang's two-stage, second order diagonally implicit RK method [48],

$$\begin{array}{c|c} \mathbf{c} & A \\ \hline & \mathbf{b^T} \end{array} = \begin{array}{c|cc} \frac{1}{4} & \frac{1}{4} & 0 \\ \frac{3}{4} & \frac{1}{2} & \frac{1}{4} \\ \hline & \frac{1}{2} & \frac{1}{2} \end{array}, \quad M = \begin{bmatrix} 0 & 0 \\ 0 & 0 \end{bmatrix}, \tag{4.2}$$

Crouzeix's two-stage, third order diagonally implicit RK method [49],

$$\begin{array}{c|c} \mathbf{c} & A \\ \hline & \mathbf{b^T} \end{array} = \begin{array}{c|cc} \frac{1}{2}+\frac{\sqrt{3}}{6} & \frac{1}{2}+\frac{\sqrt{3}}{6} & 0 \\ \frac{1}{2}-\frac{\sqrt{3}}{6} & -\frac{\sqrt{3}}{3} & \frac{1}{2}+\frac{\sqrt{3}}{6} \\ \hline & \frac{1}{2} & \frac{1}{2} \end{array}, \quad M = \left(\frac{1}{4}+\frac{\sqrt{3}}{6}\right)\begin{bmatrix} 1 & -1 \\ -1 & 1 \end{bmatrix}, \tag{4.3}$$

and the two-stage, fourth order Gauss–Legendre method [50],

$$\begin{array}{c|c} \mathbf{c} & A \\ \hline & \mathbf{b^T} \end{array} = \begin{array}{c|cc} \frac{1}{2}-\frac{\sqrt{3}}{6} & \frac{1}{4} & \frac{1}{4}-\frac{\sqrt{3}}{6} \\ \frac{1}{2}+\frac{\sqrt{3}}{6} & \frac{1}{4}+\frac{\sqrt{3}}{6} & \frac{1}{4} \\ \hline & \frac{1}{2} & \frac{1}{2} \end{array}, \quad M = \begin{bmatrix} 0 & 0 \\ 0 & 0 \end{bmatrix}. \tag{4.4}$$

These RK methods will be adopted in our numerical experiments.

The experimental orders of convergence (EOC) at $T = n\tau$ in terms of h and τ are determined respectively by

$$\text{EOC} = \log_2\left(\frac{e_h^n}{e_{h/2}^n}\right), \quad \text{EOC} = \log_2\left(\frac{e_h^n}{e_h^{2n}}\right),$$

where e_h^n represents the error between the numerical solution $u_h^n(x,y)$ and the exact solution $u(x,y,t^n)$, and e_h^{2n} corresponds to the numerical solution with $\tau/2$ as the time step.

The Swift–Hohenberg equation is a special case of model equation (1.1) with $a = 1$ and

$$\Phi(u) = -\frac{\epsilon}{2}u^2 - \frac{g}{3}u^3 + \frac{u^4}{4}, \tag{4.5}$$

that is,

$$u_t = -\Delta^2 u - 2\Delta u + (\epsilon - 1)u + gu^2 - u^3. \tag{4.6}$$

Here physical parameters are $g \geq 0$ and $\epsilon \in \mathbb{R}$, which together with the size of the domain play an important role in pattern selection; see, e.g., [51–53]. In our numerical tests, we focus on (4.5) with $g \geq 0$ and $\epsilon > 0$. This function has double wells with two local minimal values at $u_\pm = \frac{g\pm\sqrt{g^2+4\epsilon}}{2}$ such that $\Phi'(u_\pm) = 0$, and

$$\Phi(u) \geq \min\{\Phi(u_\pm)\} = \min_{v=u_\pm}\left(-\frac{1}{12}\left(gv(g^2+4\epsilon) + \epsilon(g^2+3\epsilon)\right)\right) = -b,$$

so it suffices to choose the method parameter $C_0 \geq b$. In all numerical examples $b < 1$, together with the discussion in Remark 4.1, we will take $C_0 = 10^3$ for all examples.

Example 4.1 (*Spatial Accuracy Test*)**.** Consider the Swift–Hohenberg equation (4.6) with an added source of form

$$f(x,y,t) = -\varepsilon v - gv^2 + v^3, \quad v := e^{-t/4}\sin(x/2)\sin(y/2),$$

subject to initial data

$$u_0(x,y) = \sin(x/2)\sin(y/2). \tag{4.7}$$

This problem has an explicit solution

$$u(x,y,t) = e^{-t/4}\sin(x/2)\sin(y/2). \tag{4.8}$$

Table 1
L^2, L^∞ errors and EOC at $T = 0.01$ with mesh $N \times N$.

k	τ		$N = 8$	$N = 16$		$N = 32$		$N = 64$	
			Error	Error	Order	Error	Order	Error	order
1	1e−3	$\|u - u_h\|_{L^2}$	3.73985e−01	9.73764e−02	1.94	2.39651e−02	2.02	5.95959e−03	2.01
		$\|u - u_h\|_{L^\infty}$	1.38441e−01	3.83905e−02	1.85	9.61382e−03	2.00	2.40153e−03	2.00
2	1e−4	$\|u - u_h\|_{L^2}$	7.10034e−02	1.50739e−02	2.24	2.02727e−03	2.89	2.58614e−04	2.97
		$\|u - u_h\|_{L^\infty}$	2.41033e−02	3.22536e−03	2.90	4.40302e−04	2.87	5.63426e−05	2.97
3	2e−5	$\|u - u_h\|_{L^2}$	1.20130e−02	1.13186e−03	3.41	7.72408e−05	3.87	4.94306e−06	3.97
		$\|u - u_h\|_{L^\infty}$	3.85682e−03	3.68735e−04	3.39	2.43500e−05	3.92	1.53904e−06	3.98

Table 2
L^2, L^∞ errors and EOC at $T = 1.5$ with time step τ.

RK	L		$\tau = 2^{-2}$	$\tau = 2^{-3}$		$\tau = 2^{-4}$		$\tau = 2^{-5}$	
			Error	Error	Order	Error	Order	Error	order
(4.2)	0	$\|u - u_h\|_{L^2}$	5.84575e−02	1.29975e−02	2.17	3.21365e−03	2.02	8.05270e−04	2.00
		$\|u - u_h\|_{L^\infty}$	5.51717e−03	1.13568e−03	2.28	2.80093e−04	2.02	7.04859e−05	1.99
(4.3)	2	$\|u - u_h\|_{L^2}$	6.49591e−03	7.15397e−04	3.18	8.88739e−05	3.01	9.69107e−06	3.20
		$\|u - u_h\|_{L^\infty}$	7.59053e−04	1.09547e−04	2.79	1.37766e−05	2.99	1.46945e−06	3.23
(4.4)	2	$\|u - u_h\|_{L^2}$	2.10020e−03	1.38306e−04	3.92	7.30941e−06	4.24	–	–
		$\|u - u_h\|_{L^\infty}$	3.43273e−04	2.20772e−05	3.96	1.42833e−06	3.95	–	–

To be specific, we take $\varepsilon = 0.025$, $g = 0$, and domain $\Omega = [-2\pi, 2\pi]^2$ with periodic boundary conditions. We shall test the RKDG algorithm based on the RK method with Butcher tableau (4.4) and P^k polynomials. Note that due to the source term, we need to add

$$(f(\cdot, t^n + b_i\tau), \phi),$$

to the right hand side of both (3.7)a and (3.14a). In prediction step, we take $L = 10$ and tolerance $Tol = 10^{-10}$. This example is used to test the spatial accuracy, using polynomials of degree k with $k = 1,\ 2,\ 3$ on 2D rectangular meshes. Both errors and orders of convergence at $T = 0.01$ are reported in Table 1. These results confirm the $(k+1)$th orders of accuracy in L^2, L^∞ norms.

Example 4.2 (*Temporal Accuracy Test*)**.** Consider the Swift–Hohenberg equation (4.6) with an added source of form

$$f(x, y, t) = -\varepsilon v - g v^2 + v^3, \quad v := e^{-49t/64}\sin(x/4)\sin(y/4),$$

subject to initial data

$$u_0(x, y) = \sin(x/4)\sin(y/4). \tag{4.9}$$

Its exact solution is given by

$$u(x, y, t) = e^{-49t/64}\sin(x/4)\sin(y/4).$$

We want to test the temporal accuracy of the RKDG algorithm, for which we take $\varepsilon = 0.025, g = 0$, and domain $\Omega = [-4\pi, 4\pi]^2$ with periodic boundary conditions. We apply the two-stage RKDG algorithm based on second, third and fourth order RK methods with Butcher tableau (4.2)–(4.4) and P^3 polynomials. Similar to Example 4.1, we also need to add

$$(f(\cdot, t^n + b_i\tau), \phi),$$

to the right hand side of both ((3.7)a) and (3.14a). We take time steps $\tau = 2^{-m}$ for $2 \le m \le 5$ and mesh size 64×64. In the prediction step, we choose the tolerance $Tol = 10^{-10}$ and the value of L depends on the specific RK methods. The L^2, L^∞ errors and orders of convergence at $T = 1.5$ are shown in Table 2, and these results confirm that the schemes as tested can achieve the optimal orders of convergence in time.

Example 4.3 (*Rolls and Hexagons*)**.** In this example, we simulate the formation and evolution of patterns of the Swift–Hohenberg equation (4.6), which arises in the Rayleigh–Bénard convection. Following [5,54], we run the simulation from $t = 0$ to $t = 198$ on a rectangular domain $\Omega = [0, 100]^2$, subject to random initial data and periodic boundary conditions. Model parameters $\varepsilon,\ g$ will be specified below for different cases.

We apply the RKDG algorithm based on the fourth order RK method with Butcher tableau (4.4) and P^2 polynomials using mesh 128×128. In prediction step, we take $L = 3$ and tolerance $Tol = 10^{-5}$. This example is used to test the spatial accuracy, using polynomials of degree k with $k = 1,\ 2,\ 3$ on 2D rectangular meshes. We take time step $\tau = 0.1$, which

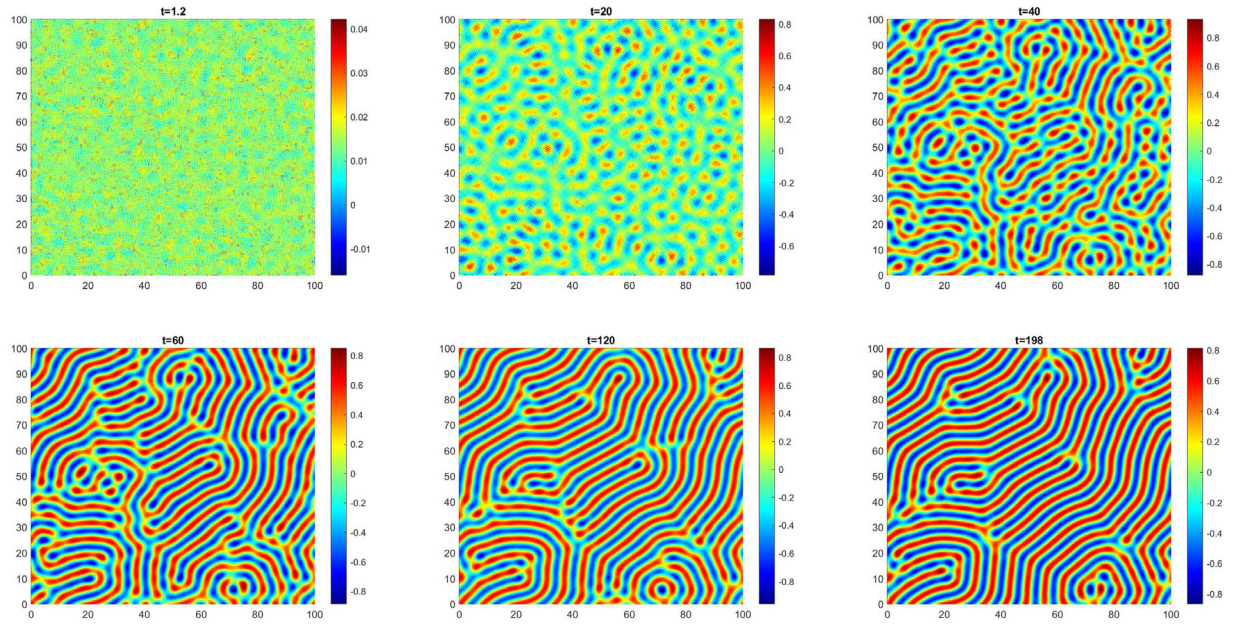

Fig. 1. Evolution of periodic rolls.

Table 3
L^∞ errors of the solutions for different L.

L	$t=0$	$t=6$	$t=20$	$t=40$	$t=60$	$t=120$	$t=150$	$t=198$
0	0	0.0479	0.4606	0.8883	1.0519	1.2442	1.2591	1.2636
1	0	0.0517	0.0566	0.0557	0.0580	0.0876	0.0878	0.0472
2	0	0.0519	0.0551	0.0491	0.0446	0.0333	0.0289	0.0232

is much larger than that used in [5,54]. In the following two test cases, we output $E(q_h^n, U_h^n) - C_0|\Omega|$ instead of $E(q_h^n, U_h^n)$ to better observe the evolution of the original free energy $\mathcal{E}(u)$.

Test case 1. (Rolls) For parameters $\varepsilon = 0.3,\ g = 0$, we observe the periodic rolls for different times as shown in Fig. 1. We see that the pattern evolves approaching the steady-state after $t > 60$, as also evidenced by the energy evolution plot in Fig. 3a.

Test case 2. (Hexagons) The numerical simulations with the parameters $\varepsilon = 0.1,\ g = 1.0$ reveal vividly the formation and evolution of the hexagonal pattern as shown in Fig. 2. The pattern at $t = 1.2$ is similar to that of rolls as shown in Fig. 1. Similar to the pattern obtained by the IEQ-DG scheme in [5], we also observe that at a certain point before $t = 40$, lines break up giving way to single droplets that take hexagonal symmetry. The steady state is approaching after $t > 100$.

The evolution of the patterns for both cases is shown to satisfy the energy dissipation law in Fig. 3. With the same parameters $\varepsilon,\ g$ as in [5], the RKDG algorithm can generate quite similar formation and evolution of both roll and hexagonal patterns even with a larger time step.

Example 4.4. We still use Example 4.3 but with focus on the evolution of the modified energy $E(q_h^n, U_h^n) - C_0|\Omega|$ in (3.4), the original energy $\mathcal{E}(u_h^n, q_h^n)$ in (2.6), and their difference

$$\left|E(q_h^n, U_h^n) - C_0|\Omega| - \mathcal{E}(u_h^n, q_h^n)\right|$$

when time step τ is not small. Again, we apply the RKDG algorithm based on the fourth order RK method with Butcher tableau (4.4) and P^2 polynomials using mesh 128×128. In the prediction step, we take tolerance $Tol = 10^{-5}$, but different number of iterations $L = 0, 1, 2$. We take the time step $\tau = 0.5$, which is larger than $\tau = 0.1$ used in Example 4.3. Below we will take the solution with smaller τ in Example 4.3 as a reference solution.

Test case 1. (Rolls) For $L = 0, 1, 2$, the L^∞ errors of the solutions with the reference solution at different t are shown in Table 3, and the pattern snapshots at $t = 40, 120, 198$ are given in Fig. 4. From these results, we still observe the roll patterns even τ is large. However, without the prediction step, namely $L = 0$, the pattern has a large error; for $L = 1, 2$, the patterns are comparable to those obtained in Example 4.3 with Test case 1.

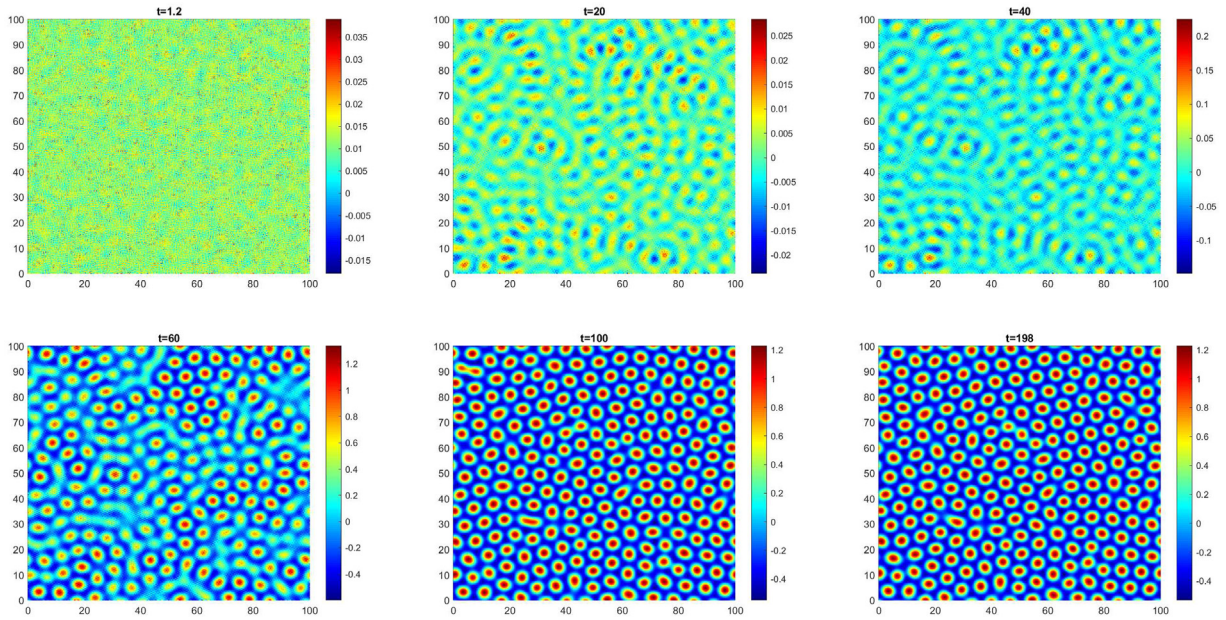

Fig. 2. Evolution of hexagonal patterns.

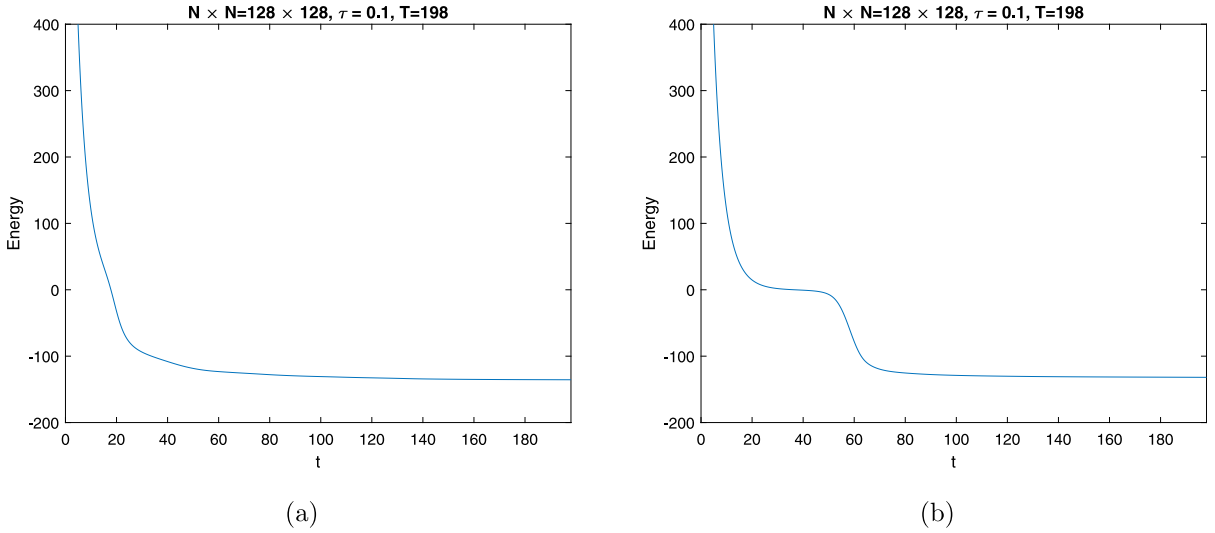

Fig. 3. Energy evolution. (a) Rolls. (b) Hexagons.

The energy comparison results are given in Fig. 5, from which we find that (1) both the modified energy and the original energy satisfy the energy dissipation law; (2) the difference between the modified energy and the original energy is large for $L = 0$, but significantly reduced when using an appropriate prediction step, with $L = 1$ or $L = 2$.

We have also conducted experiments on Test case 2 with Hexagons, the observation is entirely similar, so we omit the related results.

5. Concluding remarks

In this paper, we present a new class of arbitrarily high order, fully discrete DG schemes. These schemes have several advantageous properties: (1) the schemes are all linear such that they are easy to implement and computationally

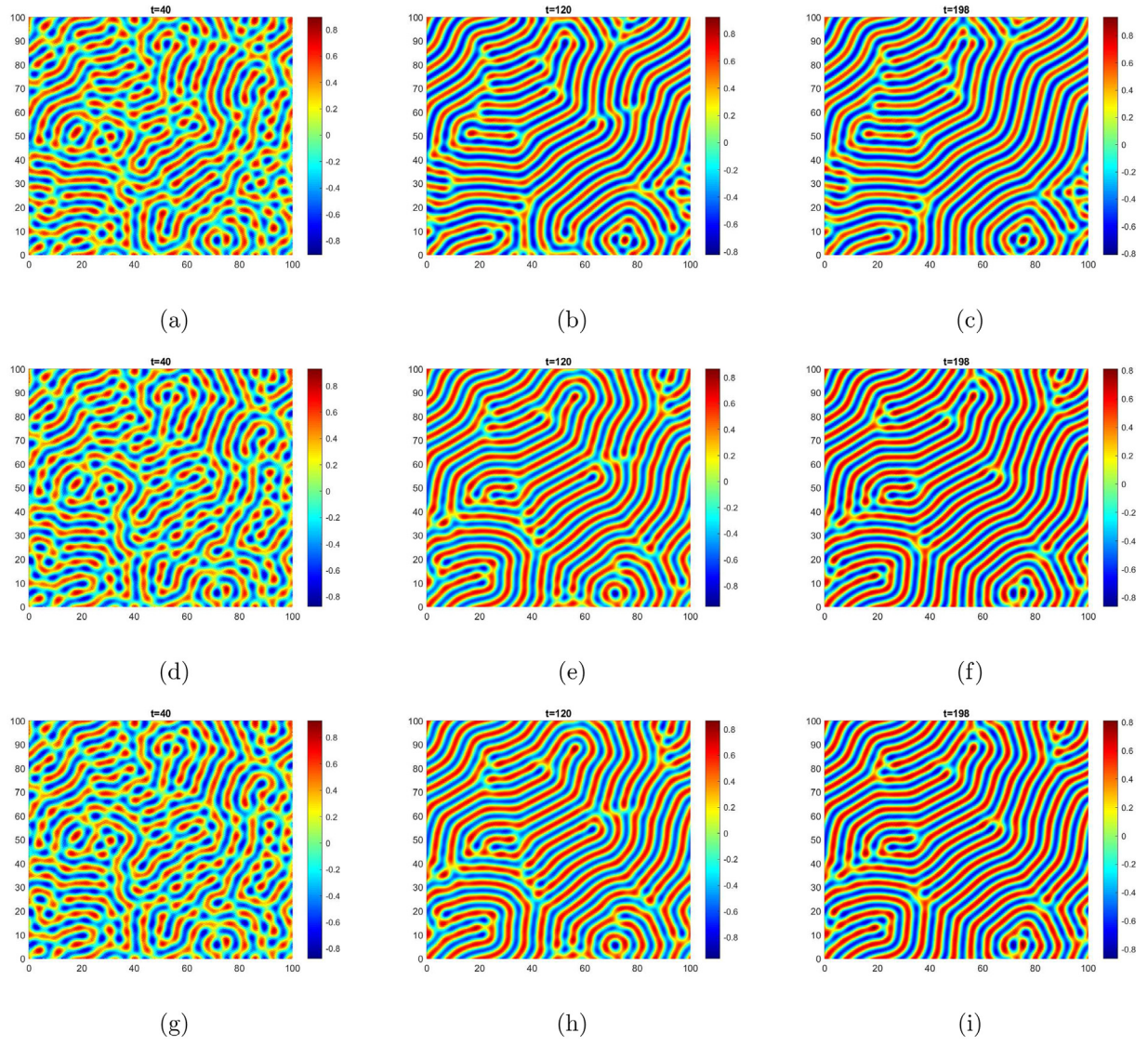

Fig. 4. Evolution of periodic rolls: (a–c) $L = 0$; (d–f) $L = 1$; (g–i) $L = 2$.

efficient; (2) the schemes are uniquely solvable and unconditionally energy stable, these ensure that large time steps can be used in long time simulations; (3) the schemes can reach arbitrarily high order of accuracy in both space and time, so that desired accuracy of solutions can be guaranteed with flexible meshes and time steps; (4) the schemes do not depend on the specific form of the DG operator explicitly, hence applicable to a larger class of semi-discrete DG schemes as long as they satisfy a semi-discrete energy dissipation law. The special structure of the DG formulation is nicely used in the proof for energy stability. In addition, the prediction step in the RKDG algorithm is shown to be helpful in resolving the issue with IEQ that the auxiliary variable deviates from its original counterpart due to numerical errors accumulated through time discretization. Several numerical examples are presented to assess the scheme performance in terms of accuracy and energy stability. The numerical results on two dimensional pattern formation problems indicate that the method is able to deliver expected patterns of high accuracy with a larger time step on coarse meshes.

Acknowledgments

This research was supported by the National Science Foundation, USA under Grant DMS1812666.

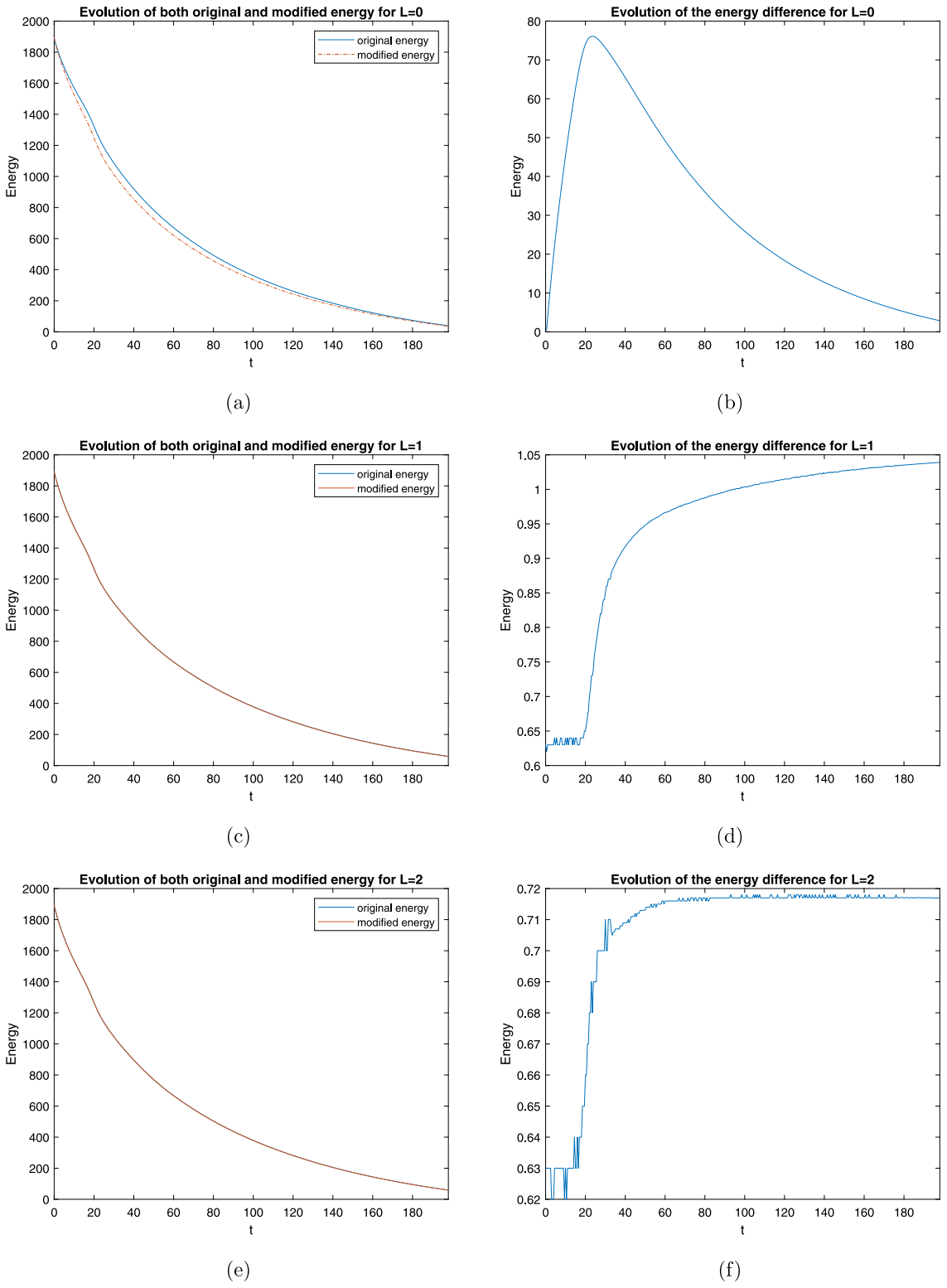

Fig. 5. Energy evolution. (a–b) $L = 0$; (c–d) $L = 1$; (e–f) $L = 2$.

References

[1] J. Swift, P.C. Hohenberg, Hydrodynamic fluctuations at the convective instability, Phys. Rev. A 15 (1977) 319–328.
[2] G. Dee, W. Saarloos, Bistable systems with propagating fronts leading to pattern formation, Phys. Rev. Lett. 60 (1988) 2641–2644.
[3] L.A. Peletier, W.C. Troy, Spatial patterns described by the extended Fisher-Kolmogorov (EFK) equation: kinks, Differential Integral Equations 8 (1995) 1279–1304.
[4] P.C. Fife, M. Kowalczyk, A class of pattern-forming models, J. Nonlinear Sci. 9 (1999) 641–669.
[5] H. Liu, P. Yin, Unconditionally energy stable DG schemes for the Swift-Hohenberg equation, J. Sci. Comput. 81 (2019) 789–819.
[6] H. Liu, P. Yin, On the SAV-DG method for a class of fourth order gradient flows, 2020, arXiv preprint, arXiv:2008.11877.
[7] C.I. Christov, J. Pontes, Numerical scheme for Swift–Hohenberg equation with strict implementation of Lyapunov functional, Math. Comput. Modelling 35 (2002) 87–99.
[8] C.I. Christov, J. Pontes, D. Walgraef, M.G. Velarde, Implicit time splitting for fourth-order parabolic equations, Comput. Methods Appl. Mech. Engrg. 148 (1997) 209–224.
[9] H. Gomez, X. Nogueira, A new space–time discretization for the swift–hohenberg equation that strictly respects the Lyapunov functional, Commun. Nonlinear Sci. Numer. Simul. 17 (12) (2012) 4930–4946.
[10] H.G. Lee, A semi-analytical Fourier spectral method for the Swift–Hohenberg equation, Comput. Math. Appl. (CMA) 74 (8) (2017) 1885–1896.
[11] A.F. Sarmiento, L.F.R. Espath, P. Vignal, L. Dalcin, M. Parsani, V.M. Calo, An energy-stable generalized-α method for the Swift–Hohenberg equation, J. Comput. Appl. Math. 344 (2018) 836–851.
[12] D.J. Eyre, Unconditionally gradient stable time marching the Cahn-Hilliard equation, in: Computational and Mathematical Models of Microstructural Evolution (San Francisco, CA, 1998), Volume 529 of Mater. Res. Soc. Sympos. Proc, MRS, 1998, pp. 39–46.
[13] X. Wu, G.J. v. Zwieten, K.G. v. d. Zee, Stabilized second-order convex splitting schemes for Cahn-Hilliard models with application to diffuse-interface tumor-growth models, Int. J. Numer. Methods Biomed. Eng. 30 (2014) 180–203.
[14] C. Xu, T. Tang, Stability analysis of large time-stepping methods for epitaxial growth models, SIAM. J. Num. Anal. 44 (2006) 1759–1779.
[15] J. Shen, X. Yang, Numerical approximations of Allen-Cahn and Cahn-Hilliard equations, Discrete Contin. Dyn. Syst. A 28 (2010) 1669–1691.
[16] X. Yang. Linear, First and second order and unconditionally energy stable numerical schemes for the phase field model of homopolymer blends, J. Comput. Phys. 302 (2016) 509–523.
[17] J. Zhao, X. Yang, Y. Gong, X. Zhao, J. Li, X. Yang, Q. Wang. Linear, Second order and unconditionally energy stable schemes for the viscous Cahn-Hilliard equation with hyperbolic relaxation, J. Comput. Appl. Math. 343 (2018) 80–97.
[18] J. Shen, J. Xu, X. Yang, The scalar auxiliary variable (SAV) approach for gradient flows, J. Comput. Phys. 353 (2018) 407–416.
[19] J. Yan, C.-W. Shu, Local discontinuous Galerkin methods for partial differential equations with higher order derivatives, J. Sci. Comput. 17 (1) (2002) 24–47.
[20] B. Dong, C.-W. Shu, Analysis of a local discontinuous Galerkin method for linear time-dependent fourth-order problems, SIAM J. Numer. Anal. 47 (5) (2009) 3240–3268.
[21] H. Wang, Q. Zhang, C.-W. Shu, Stability analysis and error estimates of local discontinuous Galerkin methods with implicit-explicit time-marching for the time-dependent fourth order PDEs, ESAIM M2AN 51 (2017) 1931–1955.
[22] X. Feng, O.A. Karakashian, Fully discrete dynamic mesh discontinuous Galerkin methods for the Cahn-Hilliard equation of phase transition, Math. Comp. 76 (2007) 1093–1117.
[23] X. Feng, Y. Li, Y. Xing, Analysis of mixed interior penalty discontinuous Galerkin methods for the Cahn-Hilliard equation and the hele-shaw flow, SIAM J. Numer. Anal. 54 (2) (2016) 825—847.
[24] G.N. Wells. E. Kuhl, K. Garikipati, A discontinuous Galerkin method for the Cahn-Hilliard equation, J. Comput. Phys. 218 (2006) 860–877.
[25] H. Liu, J. Yan, The direct discontinuous Galerkin (DDG) method for diffusion problems, SIAM J. Numer. Anal. 47 (1) (2009) 675–698.
[26] H. Liu, J. Yan, The direct discontinuous Galerkin (DDG) method for diffusion with interface corrections, Commun. Comput. Phys. 8 (3) (2010) 541–564.
[27] H. Liu, Optimal error estimates of the direct discontinuous Galerkin method for convection–diffusion equations, Math. Comp. 84 (2015) 2263–2295.
[28] Y. Cheng, C.-W. Shu, A discontinuous Galerkin finite element method for time dependent partial differential equations with higher order derivatives, Math. Comp. 77 (2008) 699–730.
[29] H. Liu, P. Yin, A mixed discontinuous Galerkin method without interior penalty for time-dependent fourth order problems, J. Sci. Comput. 77 (2018) 467–501.
[30] R.M. Kirby, T.C. Warburton, I. Lomtev, G.E.Karniadakis, A discontinuous Galerkin spectral/*hp* method on hybrid grids, Appl. Numer. Math. 33 (2000) 393–405.
[31] J.S. Hesthaven, T. Warburton, Nodal Discontinuous Galerkin Methods: Algorithms, Analysis, and Applications, Springer, New York, 2007.
[32] B. Riviére, Discontinuous Galerkin Methods for Solving Elliptic and Parabolic Equations, Society for Industrial and Applied Mathematics, 2008.
[33] C.-W. Shu, Discontinuous Galerkin methods: general approach and stability, in: Numerical Solutions of Partial Differential Equations, in: Adv. Courses Math. CRM Barcelona, Birkhäuser, Basel, 2009, pp. 149–201.
[34] L. Chen, J. Zhao, Yang. X., Regularized linear schemes for the molecular beam epitaxy model with slope selection, Appl. Numer. Math. 128 (2018) 138–156.
[35] D. Hou, M. Azaiez, C. Xu, A variant of scalar auxiliary variable approaches for gradient flows, J. Comput. Phys. 395 (2019) 307–332.
[36] Z. Liu, X. Li, Efficient modified techniques of invariant energy quadratization approach for gradient flows, Appl. Math. Lett. 98 (2019) 206–214.
[37] Z. Xu, X. Yang, H. Zhang, Z. Xie, Efficient and linear schemes for anisotropic Cahn-Hilliard model using the stabilized-invariant energy quadratization (S-IEQ) approach, Comput. Phys. Commun. 238 (2019) 36–49.
[38] Y. Gong, J. Zhao, Q. Wang, Arbitrarily high-order unconditionally energy stable SAV schemes for gradient flow models, Comput. Phys. Comm. 249 (2020) 107033.
[39] Y. Gong, J. Zhao, Q. Wang, Arbitrarily high-order unconditionally energy stable schemes for thermodynamically consistent gradient flow models, SIAM J. Sci. Comput. 42 (1) (2020) B135–B156.
[40] Y. Gong, J. Zhao, Q. Wang, Arbitrarily high-order linear energy stable schemes for gradient flow models, J. Comput. Phys. 419 (2020) 109610.
[41] H. Liu, P. Yin, Unconditionally energy stable DG schemes for the Cahn-Hilliard equation, J. Comput. Appl. Math. 390 (2021) 113375.
[42] G. Akrivis, B. Li, D. Li, Energy-decaying extrapolated RK–SAV methods for the Allen–Cahn and Cahn–Hilliard equations, SIAM J. Sci. Comput. 41 (6) (2019) A3703–A3727.
[43] S.M. Allen, J.W. Cahn, A microscopic theory for antiphase boundary motion and its application to antiphase domain coarsening, Acta. Metall. 27 (1979) 1085–1095.
[44] J.W. Cahn, J.E. Hilliard, Free energy of a nonuniform system. I. interfacial free energy, J. Chem. Phys. 28 (1958) 258–267.
[45] K. Burrage, J.C. Butcher, Stability criteria for implicit Runge–Kutta methods, SIAM J. Numer. Anal. 16 (1) (1979) 46–57.
[46] J. Zhao, A revisit of the energy quadratization method with a relaxation technique, Appl. Math. Lett. 120 (2021) 107331.

[47] M. Jiang, Z. Zhang, J. Zhao, Improving the accuracy and consistency of the scalar auxiliary variable (SAV) method with relaxation, 2021, arXiv preprint arXiv:2104.06620.
[48] M.Z. Qin, M.Q. Zhang, Symplectic Runge–Kutta algorithms for Hamiltonian systems, J. Comput. Math. (Suppl.) (1992) 205–215.
[49] S.P. Nørsett, Semi-Explicit Runge-Kutta Methods, Department of Mathematics, University of Trondheim, ISBN: 9788271510091, 1974.
[50] A. Iserles, A First Course in the Numerical Analysis of Differential Equations, Cambridge University Press, 1996.
[51] G.J.B. van den Berg, L.A. Peletier, W.C. Troy, Global branches of multi-bump periodic solutions of the Swift–Hohenberg equation, Arch. Ration. Mech. Anal. 158 (2001) 91–153.
[52] L.A. Peletier, V. Rottschäfer, Pattern selection of solutions of the Swift–Hohenberg equation, Physica D 194 (1) (2004) 95–126.
[53] D. Morgan, J.H.P. Dawes, The Swift–Hohenberg equation with a nonlocal nonlinearity, Physica D 270 (1) (2014) 60–80.
[54] S.S. Pérez-Moreno, S.R. Chavarría, G.R. Chavarría, Numerical solution of the Swift–Hohenberg equation, in: J. Klapp, A. Medina (Eds.), Experimental and Computational Fluid Mechanics, in: Environmental Science and Engineering, Springer, Cham, 2014, pp. 409–416.